Analytical solutions of one-way coupled magnetohydrodynamic free surface flow

Righolt, B. W.; Kenjeres, S.; Kalter, R.; Tummers, M. J.; Kleijn, C. R.

DOI
10.1016/j.apm.2015.09.101

Publication date
2016

Document Version
Accepted author manuscript

Published in
Applied Mathematical Modelling: simulation and computation for engineering and environmental systems

Analytical solutions of one-way coupled magnetohydrodynamic free surface flow

B. W. Righolt[a,b], S. Kenjereš[a,b], R. Kalter[a,b], M. J. Tummers[c,b], C. R. Kleijn[a,b]

[a] *Department of Chemical Engineering, Faculty of Applied Sciences, Delft University of Technology, Delft, 2628BL, Netherlands*
[b] *J. M. Burgerscentre for Fluid Mechanics*
[c] *Laboratory for Aero and Hydrodynamics, Delft University of Technology*

Abstract

We study the flow in a layer of conductive liquid under the influence of surface tension, gravity, and Lorentz forces due to imposed potential differences and transverse magnetic fields, as a function of the Hartmann number, the Bond number, the Reynolds number, the capillary number and the height-to-width ratio A. For aspect ratios $A \ll 1$ and Reynolds numbers $Re \leq A$, lubrication theory is applied to determine the steady state shape of the liquid surface to lowest order. Assuming low Hartmann ($Ha \leq O(1)$), capillary ($Ca \leq O(A^4)$), Bond ($Bo \leq O(A^2)$) numbers and contact angles close to 90°, the flow details below the surface and the free surface elevation for the complete domain are determined analytically using the method of matched asymptotic expansions. The amplitude of the free surface deformation scales linearly with the capillary number and decreases with increasing Bond number, while the shape of the free surface depends on the Bond number and the contact angle condition. The strength of the flow scales linearly with the magnetic field gradient and applied potential difference and vanishes for high aspect ratio layers ($A \to 0$). The analytical model results are confirmed by numerical simulations using a finite volume moving mesh interface tracking method, where the Lorentz force is calculated from the equation for the electric potential. It is shown that the analytical result for the free surface elevation is accurate within 0.4% from the numerical results for $Ha^2 \leq 1$, $Ca \leq A^4$, $Bo \leq A^2$, $Re \leq A$ and $A \leq 0.1$ and within 2% for $A = 0.5$. For $A = 0.1$, the solution remains accurate within 1% of the numerical solution when either Ha^2 is increased to 400, Ca to $200A^4$ or Bo to $100A^2$.

Keywords: magnetohydrodynamics, free surface, analytical solutions, numerical solutions, lubrication theory, matched asymptotic expansions

1. Introduction

Magnetohydrodynamic (MHD) free surface flow of a conductive liquid in a spatially non-uniform magnetic field is relevant to various applications in e.g. metallurgy [1, 2, 3, 4] and crystal growth processes, such as Czochralski and Bridgman growth [2, 5, 6]

Wall-bounded single phase MHD flow of a conducting liquid in a magnetic field has been the subject of many theoretical studies, e.g. pipe [7] and duct [8] flow in a uniform magnetic field, convection in a non-uniform magnetic field [9], buoyancy driven Darcy flow in a uniform magnetic field [10, 11, 12], and lubrication flow with injected currents [13]. Free surface MHD flow has been studied both theoretically and experimentally, e.g. driven by an imposed magnetic field [14], by injected currents [15, 16], or due to buoyancy [17].

In the present paper we will study the one-way coupled magnetohydrodynamic (MHD) free surface flow of a conductive fluid in a shallow, two-dimensional cavity subject to a differentially applied electric potential in a spatially non-uniform magnetic field. The Lorentz force will be the only driving force for the flow, while gravity and surface tension act as the restoring forces for the free surface deformation. We will use the analytical methods of lubrication theory and matched asymptotic expansions to determine the free surface elevation and flow inside the cavity. This combination of methods has been used previously to study flows in shallow cavities, for example in buoyancy driven single phase flow [18], and later for free surface flow driven by a Marangoni force [19]. It has also been used for single phase MHD flow [20] and free surface MHD

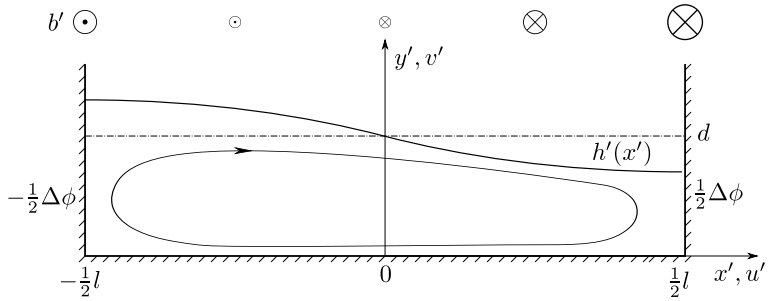

Figure 1: Schematic representation of the liquid layer, with a potential difference $\Delta\phi$ across the domain and an insulated bottom. The dash-dotted line is the undisturbed interface and the solid line $h(x)$ is the equilibrium surface position after application of a magnetic field in the direction perpendicular to the xy-plane, where the relative field strength is indicated in the top.

flow in a uniform magnetic field [21]. The combination of a free surface and a non-uniform magnetic field distinguishes our work from previous studies.

Our analytical solutions will subsequently be compared with numerical results from a finite volume based free surface, one-way coupled Navier-Stokes MHD flow solver. The free surface is modelled using a moving mesh interface tracking (MMIT) method and the electric potential in the one-way coupled MHD problem is calculated from a Poisson equation.

The goal of this paper is to (i) find asymptotic analytical solutions for the flow in a conductive layer of fluid influenced by Lorentz, gravity and surface tension forces, (ii) validate a free surface MHD flow solver in OpenFoam [22] against the obtained asymptotic analytical solutions and (iii) use the validated numerical solver to explore the parameter space, in terms of Hartmann number, capillary number, Bond number, Reynolds number and aspect ratio, for which the analytical solution is accurate. With the obtained knowledge about its accuracy and limitations, the presented asymptotic analytical solutions may subsequently serve as a benchmark for the validation of other numerical solvers for combined free surface and MHD flows.

This paper is outlined as follows. The mathematical framework is presented in section 2, this includes the derivation of the flow in the core and the free surface elevation. In section 3, the turning flow near the side walls is derived analytically. Section 4 demonstrates the applicability of the mathematical model for increasing magnetic field strengths. Section 5 introduces the numerical method used in this paper and section 6 shows the verification of the mathematical solutions by means of the numerical model.

2. Mathematical model

We consider a two-dimensional, finite-size liquid layer of width l and initial height d, as depicted in figure 1. The liquid has an electrical conductivity σ, density ρ and kinematic viscosity ν. The fluid above the liquid layer is assumed to have negligible electrical conductivity, density and viscosity. The surface tension between the two phases is denoted by γ and the downward directed gravitational force by g.

The left wall of the system is kept at a fixed electrical potential $-\frac{1}{2}\Delta\phi$, the right wall at $\frac{1}{2}\Delta\phi$ and the bottom wall is electrically insulated. A magnetic field $\mathbf{b}'/b_0 = -(\alpha z'/l)\hat{\mathbf{x}} - (1+\alpha x'/l)\hat{\mathbf{z}}$ is imposed, which in the plane of interest, the $z = 0$ plane, gives a linearly increasing magnetic field $\mathbf{b}' = -b_0\,(1+\alpha x'/l)\,\hat{\mathbf{z}}$. The Lorentz force associated with this magnetic field has a zero z-component in the $z = 0$ plane.

In equilibrium, a net current flows from the right to the left wall. This imposed current, which is closed externally, will later be shown to be an order of magnitude stronger than the induced current, and, which due to its interaction with the magnetic field, leads to a Lorentz force $\mathbf{f}' = \mathbf{j}' \times \mathbf{b}'$. This causes a net downward force on the conducting liquid, which is stronger at the right side than at the left side. This will initiate a circulating flow inside the fluid that via pressure build-up deforms the interface. Viscous, gravitational and surface tension forces act to oppose the Lorentz force.

2.1. Conservation equations

The problem will be studied from the conservation equations for mass, momentum and current, which, for an incompressible, non-Newtonian fluid, read

$$\nabla' \cdot \mathbf{u}' \quad = \quad 0, \tag{1}$$

$$\frac{\partial \mathbf{u}'}{\partial t'} + (\mathbf{u}' \cdot \nabla') \mathbf{u}' = -\frac{1}{\rho}\nabla' p' + \nu \nabla'^2 \mathbf{u}' + \frac{1}{\rho}\mathbf{j}' \times \mathbf{b}' + \mathbf{g}', \tag{2}$$

$$\nabla' \cdot \mathbf{j}' = 0. \tag{3}$$

In this set of equations, $\mathbf{u}'$ is defined as the velocity $\mathbf{u}' = u'\hat{\mathbf{x}} + v'\hat{\mathbf{y}}$ and $\mathbf{g}'$ is defined as the gravitational force $\mathbf{g}' = -g\hat{\mathbf{y}}$. The flow is not influencing the magnetic field, as the magnetic Reynolds number $Re_m = \sigma\mu u^* l \ll 1$, with μ the magnetic permeability and u^* the characteristic velocity scale. Under these conditions, the current $\mathbf{j}'$ can be deduced from the Maxwell equations via the electric potential ϕ and is defined as $\mathbf{j}' = \sigma\left(-\nabla'\phi' + \mathbf{u}' \times \mathbf{b}'\right)$ [23].

2.2. Boundary conditions

The boundary conditions at the left, right and bottom wall follow from figure 1 and are

$$\left.\begin{array}{llll} u' = v' = 0 & \phi' = -\frac{1}{2}\Delta\phi & \text{on} & x' = -\frac{1}{2}l, \\ u' = v' = 0 & \phi' = \frac{1}{2}\Delta\phi & \text{on} & x' = \frac{1}{2}l, \\ u' = v' = 0 & \phi'_{y'} = 0 & \text{on} & y' = 0. \end{array}\right\} \tag{4}$$

The subscripts denote derivatives with respect to the coordinate in the subscript.

For the interface conditions at $y' = h'(x')$ four conditions can be distinguished

(i) The kinematic condition describes the movement of the interface with the fluid. For steady state this means that the flow has to be parallel to the interface, thus [19]

$$u' h'_{x'} = v' \tag{5}$$

(ii) The tangential stress is continuous across the interface on both sides of the interface should balance. Since the surface tension γ is constant and the viscosity above the free surface is negligible, the tangential stress component at the interface is zero [19]

$$S'_{ij} n'_j t'_i = 0, \tag{6}$$

where S'_{ij} is the stress tensor $S'_{ij} = -p'\delta_{ij} + \mu\left(u'_i, j + u'_j, i\right)$, $\mathbf{n}'$ the surface unit normal vector and $\mathbf{t}'$ the vector tangential to the surface.

(iii) The normal component is balanced by surface tension [19]:

$$S'_{ij} n'_j n'_i = \gamma K, \tag{7}$$

with K the curvature of the surface, determined by $K = \nabla \cdot n' = h'_{x'x'}/(1 + h'_{x'})^{3/2}$. (iv) The interface can be regarded as an insulated boundary, which means that

$$j'_i n'_i \tag{8}$$

where $\hat{\mathbf{n}}$ is the unit surface normal vector.

2.3. Other constraints

Some additional constraints can be identified [19]. As the system is in a steady state, there will be no net flow passing any plane, such that

$$\int_0^{h'(x')} u'(x', y') dy' = 0. \tag{9}$$

Furthermore, the mass of the layer of liquid is conserved, thus

$$\int_{-\frac{1}{2}l}^{\frac{1}{2}l} h'(x') dx' = ld. \tag{10}$$

Finally the contact point behaviour at the three-phase point has to be described. For a contact angle θ, this reads

$$h'_{x'}\left(\pm\frac{1}{2}l\right) = \mp \tan\left(\theta - \frac{\pi}{2}\right). \tag{11}$$

2.4. Lubrication theory

To solve this problem, we follow the approach by Cormack et al. [24] and Sen and Davis [19]. The analytical solutions to the model equations are obtained by using the lubrication theory strategy, which is valid for fluid layers with a small aspect ratio (i.e. $A = d/l \to 0$). By use of matched asymptotic expansions, we will first derive a solution for the deformed interface location under the influence of a non-uniform Lorentz force, where surface tension and gravity act as a restoring force. Secondly, we will derive the flow structure of the turning flow in the side wall region.

We will solve this problem in dimensionless, lubrication type variables,

$$\begin{aligned} x' = lx, \qquad y' = dy, \qquad h' = dh, \qquad u' = u^* u, \\ v' = Au^* v, \qquad p' = \frac{\mu u^* l}{d^2} p, \qquad b' = b_0 b, \qquad \phi' = (\Delta\phi)\phi. \end{aligned} \tag{12}$$

Here the non-primed variables are the lubrication type variables. x and y are the horizontal and vertical coordinates respectively, h is the free surface elevation, u and v are the horizontal and vertical velocity components, b is the perpendicular component of the magnetic field and ϕ the electric potential. b_0 is the magnetic field strength in the centre of the cavity ($x = 0$) and the characteristic velocity u^* is defined as

$$u^* = \frac{\sigma \Delta\phi b_0 \alpha d}{\rho\nu} A, \tag{13}$$

which follows from the balance between viscous and Lorentz forces.

The system is in a steady, two-dimensional motion. In lubrication variables and using $A = d/l$, the conservation equations reduce to:

$$u_x + v_y = 0, \tag{14}$$

$$ReA^2 \left(uu_x + vu_y\right) = -Ap_x + A^3 u_{xx} + Au_{yy} - \frac{1}{\alpha}\left(\phi_y + Ha^2 Aub\right) b, \tag{15}$$

$$ReA^3 \left(uv_x + vv_y\right) = -p_y + A^4 v_{xx} + A^2 v_{yy} + A\frac{1}{\alpha}\left(\phi_x - Ha^2 Avb\right) b - A\frac{Bo}{Ca}, \tag{16}$$

$$A^2\phi_{xx} + \phi_{yy} = Ha^2\left[A^3 (vb)_x - A(ub)_y\right]. \tag{17}$$

In this context, the Reynolds number, Re, the Hartmann number, Ha, the Bond number, Bo and the capillary number Ca, are defined as

$$Re = \frac{u^* d}{\nu}, \qquad Ha^2 = \frac{\sigma b_0^2 d^2 \alpha}{\rho\nu}, \qquad Bo = \frac{\rho g d^2}{\gamma}, \qquad Ca = \frac{\rho\nu u^*}{\gamma}. \tag{18}$$

In order to eliminate the pressure from the conservation equations, we introduce the stream function ψ, which obeys the continuity equation (equation 14)

$$u = \psi_y, \qquad v = -\psi_x, \tag{19}$$

such that a single equation, similar to the one reported by Sen and Davis [19], in ψ remains instead of equations for the horizontal and vertical momentum (equations 15 and 16):

$$\begin{aligned} &ReA^2\left[\psi_y\psi_{xyy} - \psi_x\psi_{yyy} - A^2\left(\psi_x\psi_{xxy} - \psi_y\psi_{xxx}\right)\right] \\ &= A\psi_{yyyy} + 2A^3\psi_{xxyy} + A^5\psi_{xxxx} \\ &-\frac{1}{\alpha}\left[\phi_{yy}b + A^2\left(\phi_{xx}b + \phi_x b_x\right) + Ha^2 A\left(\psi_{yy}b^2 + A^2\psi_{xx}b^2 + 2A^2\psi_x b b_x\right)\right], \end{aligned} \tag{20}$$

and for the charge conservation equation

$$A^2\phi_{xx} + \phi_{yy} = -Ha^2\left(A^3\psi_{xx}b + A^3\psi_x b_x + A\psi_{yy}b\right). \tag{21}$$

The wall boundary conditions in lubrication variables reduce to:

$$\left.\begin{array}{llll} \psi_x = \psi_y = 0 & \phi = -\frac{1}{2} & \text{on} & x = -\frac{1}{2}, \\ \psi_x = \psi_y = 0 & \phi = \frac{1}{2} & \text{on} & x = \frac{1}{2}, \\ \psi_x = \psi_y = 0 & \phi_y = 0 & \text{on} & y = 0. \end{array}\right\} \tag{22}$$

The interface conditions can be rewritten in terms of the lubrication variables
(i) The kinematic condition,

$$\psi_y h_x = -\psi_x \tag{23}$$

(ii) Continuity of the tangential stress component follows from rewriting equation 6 to

$$2h'_{x'}(v'_{y'} - u'_{x'}) + (1 - h'^2_{x'})(v'_{x'} + u'_{y'}) = 0, \tag{24}$$

which then reduces to

$$-4A^2 h_x \psi_{xy} + (1 - A^2 h_x^2)(\psi_{yy} - A^2 \psi_{xx}) = 0. \tag{25}$$

(iii) Continuity of the normal stress component follow from rewriting equation 7

$$\gamma \frac{h'_{x'x'}}{\sqrt{1 + h'^2_{x'}}} = \left[(-p' + 2\mu u'_{x'})h'^2_{x'} + (-p' + 2\mu v'_{y'}) - 2\mu(u'_{y'} + v'_{x'})h'_{x'}\right], \tag{26}$$

and then reduces to

$$Ca^{-1} A^3 h_{xx}(1 + A^2 h_x^2)^{-3/2} = -p + 2A^2(1 + A^2 h_x^2)^{-1}\left[-\psi_{xy} - h_x \psi_{yy} + A^2 h_x(\psi_{xx} + h_x \psi_{xy})\right]. \tag{27}$$

The modified pressure p_m is introduced to eliminate the hydrostatic pressure from the Navier-Stokes equation 16, such that

$$p_m = p + A\frac{Bo}{Ca}(y - 1), \tag{28}$$

where $-ABo/Ca$ is a reference pressure. Boundary condition 27, results in

$$\begin{aligned} A^3 h_{xx}(1 \quad &+ \quad A^2 h_x^2)^{-3/2} = -Ca\, p_m + ABo(h - 1) \\ &+ \quad 2A^2(1 + A^2 h_x^2)^{-1}\left[-\psi_{xy} - h_x \psi_{yy} + A^2 h_x(\psi_{xx} + h_x \psi_{xy})\right]. \end{aligned} \tag{29}$$

(iv) The electrical insultation condition

$$A^2 \phi_x h_x - \phi_y = (Au + A^3 h_x v)b. \tag{30}$$

For the additional constraints in lubrication variables we find for the steady flow condition, mass conservation and the contact angle requirement, respectively

$$\int_0^{h(x)} u(x,y)dy = 0, \tag{31}$$

$$\int_{-\frac{1}{2}}^{\frac{1}{2}} h(x)dx = 1, \tag{32}$$

$$h_x\left(\pm\frac{1}{2}\right) = \mp A^{-1}\tan\left(\theta - \frac{\pi}{2}\right). \tag{33}$$

2.5. Solution strategy

The system of equations is now reduced to two equations with unknowns ψ and ϕ. The solution strategy will be based on the method of matched asymptotic expansions [25], where we encounter boundary layers in the side wall regions near $x = \pm\frac{1}{2}$, where the flow turns. We will be looking for a solution where the flow is in the x-direction only in the lowest order far from the side walls near $x = 0$. To obtain the expression that is valid in the region far away from the wall, the stream function will be expanded as

$$\psi = \sum_{n=0}^{\infty} A^n \psi_n(x,y), \tag{34}$$

where a similar expansion can be used for the pressure p, the electric potential ϕ and the interface deformation $h(x) = \sum_{n=0}^{\infty} A^n h_n(x)$, where $h_0 = 1$ is the undisturbed interface.

For the dimensionless parameters we will use the following asymptotic limits

$$Re = \overline{Re}A, \qquad Ha^2 = \overline{Ha^2}, \tag{35}$$

where $\overline{Re}$ and $\overline{Ha^2}$ are of order $O(1)$, and thus $Re = O(A)$ and $Ha^2 = O(1)$. It should be noted that the obtained results will be equally valid for $Re < O(A)$ and the presented analytic derivation will be applicable for $Ha^2 < O(1)$ as well.

To obtain the equation for the lowest order stream function ψ_0, the assumptions in equations 34 and 35 are used together with equations 17 and 20. This gives

$$\psi_{0yyyy} = \frac{1}{\alpha}\left(\phi_{1yy}b + \overline{Ha^2}\psi_{0yy}b^2\right), \qquad \phi_{1yy} + \overline{Ha^2}\psi_{0yy}b = 0. \tag{36}$$

It should be noted that the lowest order equation for the stream function contains higher order terms, which can be eliminated by means of the higher order equations of the electric potential, thus:

$$\psi_{0yyyy} = 0, \qquad \phi_{0yy} = 0. \tag{37}$$

The boundary conditions

$$\left.\begin{array}{lll} \psi_0 = \psi_{0y} = \phi_{0y} = 0 & \text{on} & y = 0, \\ \psi_0 = \psi_{0yy} = \phi_{0y} = 0 & & \\ h_{1xx} = -\overline{Ca}p_{m0} + \overline{Bo}h_1 & \text{on} & y = 1 + Ah_1, \end{array}\right\} \tag{38}$$

are obtained from no-slip and electrically insulating conditions (equation 22), steady state condition (equation 31) and by substituting the asymptotic expansions for the free surface, where the following asymptotic limit is used (with $\overline{Ca} = O(1)$, $\overline{Bo} = O(1)$):

$$Ca = \overline{Ca}A^4, \qquad Bo = \overline{Bo}A^2 \tag{39}$$

thus $Ca = O(A^4)$ and $Bo = O(A^2)$. However, the derivation is also valid for $Ca \leq A^4$. Bo can appear in the equations to any order, as it is competing with surface tension as the restoring force. Using these assumptions, the surface tension and gravity force will turn out to first act at the same order of magnitude of the asymptotic expansions. For smaller Bond numbers, surface tension dominates the restoring force, while for larger Bond number gravity will dominate as a restoring force.

For ψ_0 we will get $\psi_0 = 0$, while for the solution of the lowest order electric potential, it can be seen that the solution $\phi_0 = x$ satisfies the Poisson equation for the electric potential as well as the boundary conditions at the outer walls, the bottom wall and the free surface. It follows that $p_0 = 0$ and thus $h_1 = 0$. Also, at this lowest order of magnitude, the current is solely composed of the injected current, which is therefore at least an order of magnitude larger than the induced currents.

This result has implications for the limiting case $A = 0$. In the case of an infinitely wide or very thin layer, the zeroth order solution will be the only term remaining, as all terms of $O(A)$ and higher vanish. Thus, in this case, the electromagnetic forces will not cause flow in the domain. In this paper we study bounded domains with $0 < A \ll 1$, such that higher order terms should be included. Progressing to the first order solution, we obtain

$$\psi_{1yyyy} = \frac{1}{\alpha}\left(\phi_{2yy}b + \overline{Ha^2}\psi_{1yy}b^2 + \phi_{0xx}b + \phi_{0x}b_x\right), \tag{40}$$

$$\phi_{0xx} + \phi_{2yy} = -\overline{Ha^2}\psi_{1yy}b, \tag{41}$$

which, with known b and ϕ_0, simplifies to

$$\psi_{1yyyy} = \frac{1}{\alpha}\phi_{0x}b_x = -1. \tag{42}$$

Subject to the boundary conditions at the bottom wall and top free surface (equations 22-23)

$$\left.\begin{array}{lll} \psi_1 = \psi_{1y} = 0 & \text{on} & y = 0, \\ \psi_1 = \psi_{1yy} = 0 & \text{on} & y = 1 + Ah_1 + A^2 h_2, \end{array}\right\} \tag{43}$$

this gives

$$\psi_1(x,y) = -\frac{1}{48} y^2 \left(2y^2 - 5y + 3\right). \tag{44}$$

Reintroducing the pressure by means of equations 15 and 16 allows to solve for the pressure, which reads

$$p_{m1} = -\frac{1+\alpha x}{\alpha}\left(y - \frac{5}{8}\right) + p_{ref}, \tag{45}$$

where p_{ref} is the reference pressure.

The boundary condition at $y = 1 + Ah_1(x) + A^2 h_2(x)$, based on the modified pressure p_{m1} reads, where p_{ref} is eliminated in favor of a different integration constant,

$$h_{2xxx} = -\overline{Ca} p_{m1x} + \overline{Bo} h_{2x}, \tag{46}$$

$$h_{2xxx} = \frac{3}{8}\overline{Ca} + \overline{Bo} h_{2x}. \tag{47}$$

This third order differential equation in h_2, gives the general solution

$$h_2(x) = \frac{1}{\sqrt{\overline{Bo}}}\left(\lambda_1 e^{\sqrt{\overline{Bo}}x} + \lambda_2 e^{-\sqrt{\overline{Bo}}x}\right) - \frac{3\overline{Ca}}{8\overline{Bo}}x + \lambda_3, \tag{48}$$

with λ_1, λ_2 and λ_3 constants that will follow from the matching condition with the boundary layer flow and the other constraints.

3. Side wall flow

It follows from equation 44, following the approach by Sen and Davis [19], that the flow in the central part of the domain is strictly horizontal ($v = 0$). This core flow solution breaks down near the vertical side walls, where the liquid has to change direction. To study this boundary layer behaviour, the stretching coordinate ξ is introduced as

$$\xi = \frac{x + \frac{1}{2}}{A^\kappa}, \tag{49}$$

which is the boundary layer coordinate for the left hand wall at $x = -\frac{1}{2}$. Realising that for derivatives in general $f_x = f_\xi A^{-\kappa}$ it follows from equation 20 that there is a significant degeneration for $\kappa = 1$, such that $\xi = A^{-1}(x + \frac{1}{2})$ and for derivatives $f_x = f_\xi A^{-1}$.

We will denote the variables in terms of the stretched coordinates for the left side wall by a tilde ($\widetilde{}$). The magnetic field $b = -(1 + \alpha x)$ is then expressed as $\widetilde{b} = (-1 + \frac{1}{2}\alpha) - A\alpha\xi = \widetilde{b}_0 + A\widetilde{b}_1$ and the equation for the stream function ψ (equation 20) as

$$\begin{aligned} &\overline{Re} A^2 \left(\widetilde{\psi}_y \widetilde{\psi}_{\xi yy} - \widetilde{\psi}_\xi \widetilde{\psi}_{yyy} - \widetilde{\psi}_\xi \widetilde{\psi}_{\xi\xi y} + \widetilde{\psi}_y \widetilde{\psi}_{\xi\xi\xi}\right) \\ &= A\nabla^4 \widetilde{\psi} - \frac{1}{\alpha}\left[\widetilde{b}\nabla^2 \widetilde{\phi} + \widetilde{b}_\xi \widetilde{\phi}_\xi + \overline{Ha^2} A \left(\widetilde{b}^2 \nabla^2 \widetilde{\psi} + 2\widetilde{\psi}_\xi \widetilde{b}\, \widetilde{b}_\xi\right)\right], \end{aligned} \tag{50}$$

where the ∇ operator is defined in terms of the stretched coordinate ξ and y, giving the Laplacian operator $\nabla^2 f = f_{\xi\xi} + f_{yy}$ and the biharmonic operator $\nabla^4 f = f_{\xi\xi\xi\xi} + 2f_{\xi\xi yy} + f_{yyyy}$.

The conservation of current evolves, as a result of stretching, into

$$\nabla^2 \widetilde{\phi} = -\overline{Ha^2} A \left(\widetilde{b}\nabla^2 \widetilde{\psi} + \widetilde{b}_\xi \widetilde{\psi}_\xi\right). \tag{51}$$

Expanding the side wall stream function $\widetilde{\psi}$ similar to the core flow ψ

$$\widetilde{\psi} = \sum_{n=0}^{\infty} A^n \widetilde{\psi}_n(x,y), \tag{52}$$

leads to an equation for the leading order stream function in the left wall boundary layer $\widetilde{\psi}_0$

$$\nabla^4\widetilde{\psi}_0 = \frac{1}{\alpha}\left[\widetilde{b}_0\nabla^2\widetilde{\phi}_1 + \widetilde{b}_1\nabla^2\widetilde{\phi}_0 + \widetilde{b}_{1\xi}\widetilde{\phi}_{0\xi} + \widetilde{b}_{0\xi}\widetilde{\phi}_{1\xi} + \overline{Ha^2}\left(\widetilde{b}_0^2\nabla^2\widetilde{\psi}_0 + 2\widetilde{b}_0\widetilde{b}_{0\xi}\widetilde{\psi}_{0\xi}\right)\right]. \tag{53}$$

Simultaneously we obtain from the charge conservation equation

$$\nabla^2\widetilde{\phi}_0 = 0, \tag{54}$$

$$\nabla^2\widetilde{\phi}_1 = -\overline{Ha^2}\left(\widetilde{b}_0\nabla^2\widetilde{\psi}_0 + \widetilde{b}_{0\xi}\widetilde{\psi}_{0\xi}\right), \tag{55}$$

which, together with $\widetilde{b}_{0\xi} = 0$, reduces equation 53 to

$$\nabla^4\widetilde{\psi}_0 = 0. \tag{56}$$

Using boundary conditions 22 and 23 and matching with ψ_0, this has the solution $\widetilde{\psi}_0 = 0$, which agrees with the observation for the core flow. When the contact angle boundary condition is limited to

$$\tan(\theta - \tfrac{1}{2}\pi) = mA^2, \tag{57}$$

the boundary condition for the free surface gives $\widetilde{h}_{1\xi\xi} = 0$ and $\widetilde{h}_{1\xi}(0) = 0$. Thus, for the free surface deformation it is obtained that $\widetilde{h}_1 = 0$.

It is observed that $\phi = x$ relates to $\widetilde{\phi}_0 = -\frac{1}{2}$ and $\widetilde{\phi}_1 = \xi$, which is satisfying the above problem. Using $\widetilde{\psi}_0 = 0$, the first order stream function $\widetilde{\psi}_1$ obeys

$$\begin{aligned}\nabla^4\widetilde{\psi}_1 = \quad & \frac{1}{\alpha}\left[\widetilde{b}_0\nabla^2\widetilde{\phi}_2 + \widetilde{b}_1\nabla^2\widetilde{\phi}_1 + \widetilde{b}_{1\xi}\widetilde{\phi}_{1\xi} + \widetilde{b}_{0\xi}\widetilde{\phi}_{2\xi}\right. \\ & \left. + \overline{Ha^2}\left(2\widetilde{b}_0\widetilde{b}_1\nabla^2\widetilde{\psi}_0 + \widetilde{b}_0^2\nabla^2\widetilde{\psi}_1\right)\right].\end{aligned} \tag{58}$$

Reducing this with relation $\nabla^2\widetilde{\phi}_2 = -\overline{Ha^2}\left(\widetilde{b}_1\nabla^2\widetilde{\psi}_0 + \widetilde{b}_0\nabla^2\widetilde{\psi}_1\right)$ from charge conservation results in

$$\nabla^4\widetilde{\psi}_1 = \frac{1}{\alpha}\widetilde{b}_{1\xi}\widetilde{\phi}_{1\xi} = -1, \tag{59}$$

which ultimately describes the change of flow direction in the boundary layer flow near the left wall.

For the outer flow, the walls at the side and bottom are no-slip, meaning $\widetilde{\psi}_1 = \widetilde{\psi}_{1y} = 0$ at the bottom and $\widetilde{\psi}_1 = \widetilde{\psi}_{1\xi} = 0$ at the left wall. For the free surface $\widetilde{\psi}_1 = 0$ (from equation 31), $\widetilde{\psi}_{1\xi} = 0$ (from equation 23) and $\widetilde{\psi}_{1yy} - \widetilde{\psi}_{1\xi\xi} = 0$ (from equations 25, 27 and 30), effectively reducing at this order to $\widetilde{\psi}_1 = \widetilde{\psi}_{1yy} = 0$. The solution for $\xi \to \infty$ should match with the core flow solution (equation 44).

The derivation for the right wall flow can be obtained following the exact same arguments, but with the stretching coordinate $\zeta = A^{-1}(\frac{1}{2} - x)$, and leads to the same results as the left wall. This will not be repeated here.

A final boundary condition for the top surface is obtained from equation 27

$$\widetilde{h}_{2\xi\xi} = 0, \tag{60}$$

Combining this with the contact angle boundary condition 33, $\widetilde{h}_{2\xi} = m$ (and similarly for the right wall) and the volume conserving property (equation 32), this leads to a closed expression for the free surface elevation that is valid over the full width of the liquid layer:

$$h_2(x) = \frac{1}{\sqrt{\overline{Bo}}}\left[\frac{3\overline{Ca}}{8\overline{Bo}}\frac{\sinh\left(\sqrt{\overline{Bo}}x\right)}{\cosh\left(\frac{1}{2}\sqrt{\overline{Bo}}\right)} - m\frac{\cosh\left(\sqrt{\overline{Bo}}x\right)}{\sinh\left(\frac{1}{2}\sqrt{\overline{Bo}}\right)}\right] - \frac{3\overline{Ca}}{8\overline{Bo}}x + \frac{2m}{\overline{Bo}}, \tag{61}$$

From equation 44 we see that the dimensionless flow strength does not scale with dimensionless parameters, while the free surface elevation depends on $\overline{Ca}$ and $\overline{Bo}$ as well. This has as an interesting consequence that, for example, the velocities in the liquid layer can be increased at fixed free surface elevation, or vice versa.

In the absence of gravity, e.g. $Bo = 0$, equation 47 would simplify to $h_{2xxx} = 3/8\overline{Ca}$, with solution

$$h_2(x) = \frac{1}{16}\overline{Ca}\left(x^3 - \frac{3}{4}x\right) - m\left(x^2 - \frac{1}{12}\right), \tag{62}$$

which is consistent with equation 61, in the limit for $Bo \to 0$. For decreasing influence of surface tension, in other words, for increasing Ca, the linear term in equation 61 will become dominant. However, the limit $Ca \to \infty$ does not exist, as close enough to the side walls, surface tension is always significant.

Reducing equation 62, for a 90° contact, e.g., $m = 0$, to units carrying a dimension, gives

$$\Delta h' = A^2 dh_2 = \frac{Cad\alpha}{16A^2}\left(\frac{x'^3}{l^3} - \frac{3}{4}\frac{x'}{l}\right) = \frac{\sigma\Delta\phi b_0 dl\alpha}{\gamma}\left(\frac{x'^3}{l^3} - \frac{3}{4}\frac{x'}{l}\right), \tag{63}$$

The horizontal velocity profile in dimensioned variables, follows from the stream function for the core flow (equation 44):

$$u'(y') = -\frac{1}{48}Au^*\left(8\frac{y'^3}{d^3} - 15\frac{y'^2}{d^2} + 6\frac{y'}{d}\right). \tag{64}$$

For a typical liquid steel ($\rho = 10^4 kg/m^3$, $\nu = 10^{-6}m^2/s$, $\sigma = 10^6 S/m, \gamma = 2N/m$) filled cavity ($d = 1mm$, $l = 10mm$) and moderate electromagnetic forcing ($b_0 = 0.01T$, $\Delta\phi = 10\mu V$, $\alpha = 2$), this leads to a characteristic velocity (equation 13) $u^* = 1mm/s$ and deformation $\Delta h' = 1\mu m$, with $Re = 20$, $Ha^2 = 0.02$, $Ca = 0.1$ and $Bo = 5$.

3.1. Turning flow in the side wall region

For the solution in the side wall region to the biharmonic equation 59, Sen and Davis [19] resort to a numerical approximation with a finite-difference approach, by discretizing the biharmonic operator with a 13-point stencil. Cormack et al. [24] show that the solution can be written in the form of an infinite sum of Papkowich-Fadle eigenfunctions. This approach, as also outlined by Benthem [26], can not be applied here, since the matching condition for $\xi \to \infty$ is not symmetric in y. We will therefore apply a related approach, which also allows for non-symmetric matching conditions.

By means of the transformation

$$\chi(\xi, y) = \widetilde{\psi}_1 - \psi_1(y), \tag{65}$$

we can reduce the biharmonic equation to

$$\nabla^4\chi = 0. \tag{66}$$

The boundary and matching conditions are summarized as

$$\left.\begin{array}{ll} \chi = \chi_y = 0 & \text{on } y = 0, \\ \chi = \chi_{yy} = 0 & \text{on } y = 1, \\ \chi(0,y) = \dfrac{1}{24}y^4 - \dfrac{5}{48}y^3 + \dfrac{1}{16}y^2, \chi_\xi = 0 & \text{on } \xi = 0, \\ \chi = \chi_\xi = 0 & \text{for } \xi \to \infty. \end{array}\right\} \tag{67}$$

The function $\chi(0, y)$ will be expanded as a Fourier sine series (or half-range expansion, as $\chi(0, 0) = 0$) according to

$$\chi(0,y) = \sum_{n=1}^{\infty} b_n \sin(n\pi y) \qquad b_n = 2\int_0^1 \chi(0,y)\sin(n\pi y)dy. \tag{68}$$

At $\xi = 0$, the second and third derivative are unknown, but essential in the further analytical derivation. These functions will also be expressed in terms of a Fourier sine series, with unknown coefficients c_n and d_n.

$$\frac{\partial^2\chi}{\partial\xi^2}(0,y) = \sum_{n=1}^{\infty} c_n \sin(n\pi y) \qquad \frac{\partial^3\chi}{\partial\xi^3}(0,y) = \sum_{n=1}^{\infty} d_n \sin(n\pi y), \tag{69}$$

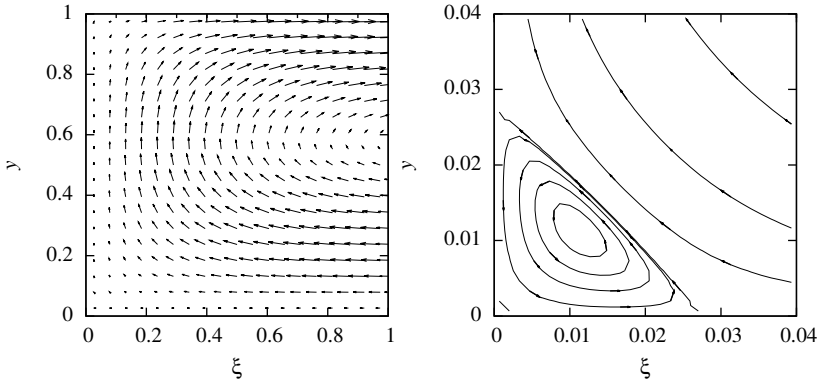

Figure 2: The velocity vector plot (left) in the left side wall region is depicted, which is derived from the side wall stream function (equation 72) for $P = 2048$. The flow is turning clockwise, while the velocity at the left and bottom boundary is zero and the top boundary is a free surface. The streamline plot (right) is determined for $P = 8192$ shows isocontours of the stream function in the region of the lower left corner of the domain, demonstrating the existence of a counter-rotating eddy in the corner.

The Laplace transform of equation 65, with f denoting the Laplace transform of χ, will reduce to a fourth order ordinary differential equation

$$\frac{\partial^4 f}{\partial y^4} + 2p^2 \frac{\partial^2 f}{\partial y^2} + p^4 f = \sum_{n=1}^{\infty} \beta_n(p) \sin(n\pi y) \qquad \beta_n(p) = \frac{\left(p^3 - 2pn^2\pi^2\right) b_n + pc_n + d_n}{\left(p^2 - n^2\pi^2\right)^2}, \tag{70}$$

Solving the differential equations subject to the given boundary conditions results in

$$f(p,y) = \sum_n \beta_n(p) \tag{71}$$
$$\left[\sin(n\pi y) + \frac{n\pi}{p - \cos p \sin p} \left(-\sin(py) + \sin^2 p \sin(py) y + \sin p \cos p \cos(py) y\right)\right]$$

The inverse Laplace transform can be obtained by a complex contour integration and by application of Jordan's lemma and the Cauchy residue theorem. The coefficients c_n and d_n are calculated up to $n = P$ by requiring the residues of $2P$ poles p_k of $f(p,y)$ $(2p - \sin 2p = 0)$ with $\mathrm{Re}(p_k) > 0$ to vanish, such that

$$\chi(\xi, y) = \sum_{k=1}^{2P} \sum_{n=1}^{P} n\pi \beta_n(-p_k) F(-p_k, y) e^{-p_k \xi}, \tag{72}$$

with

$$F(p_k, y) = \frac{-\sin(p_k y) + \sin^2 p_k \sin(p_k y) y + \sin p_k \cos p_k \cos(p_k y) y}{2 \sin^2 p_k}. \tag{73}$$

The back transformation from χ to $\widetilde{\psi}_1$ now follows from equation 65.

The solution up to $P = 8192$ is obtained by first finding the poles in the first quadrant numerically, following the method outlined by Meylan and Gross [27] and the knowledge that the poles in the complex plane can be found on the curve $x^2 = \cosh^2 y - y^2 \coth^2 y$ for $p = x + iy$. Then, the coefficients c_n and d_n are determined by Gauss-Jordan elimination of the full matrix of size $2P \times 2P$. Figure 2 shows the currently obtained velocity field for $P = 2048$ and streamlines in the region close to the corner for $P = 8192$. A counter-rotating eddy was found close to the corner, as was predicted by Moffatt [28]. Such a counter-rotating eddy was not found in the corner near the free surface.

Figure 3 shows the velocity magnitude along the line $\xi = y$, where a different number of poles are included to calculate the stream function. It shows the convergence of the velocity magnitude with an increasing number of poles. It can be seen that increasing the amount of poles above 4 does not change the velocity profile beyond a distance of 0.1 from the corner, while $P = 1024$ and $P = 8192$ are enough for an accurate velocity profile beyond a distance of 0.01 and 0.002 respectively.

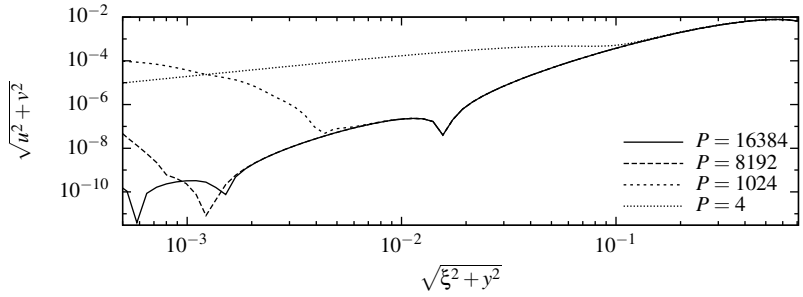

Figure 3: The velocity magnitude along the line $\xi = y$ in figure 2, which shows the effect of increasing the amount of poles (see equation 72) on the velocity magnitude for $P = 4$, $P = 1024$, $P = 8192$ and $P = 16384$.

The minimum in this velocity profile is related to the centre of the eddy. Increasing the number of poles reveals a secondary minimum, which is an indication for the second eddy of the infinite series of eddies in the corner, as predicted by Moffatt [28].

4. Increased magnetic interaction

In the derivation of the free surface elevation (equation 61), it was found that for the Hartmann number $Ha = O(1)$, only $O(A)$ flow is present. Suppose the square of the Hartmann number increases by an order in A, thus $Ha^2 = \overline{Ha^2}A^{-1}$. higher Hartmann number, it can be shown that, again, $\psi_0 = 0$ and the core flow ψ_1, can be solved by

$$\psi_{1yyyy} = -1, \qquad \psi_1 = -\frac{1}{48}y^2\left(2y^2 - 5y + 3\right), \tag{74}$$

which would result in the general solution for h_2 as given by equation 48.

For the side wall solution, again $\widetilde{\psi}_0 = 0$ is found, however, at higher order

$$\nabla^4\widetilde{\psi}_1 = \frac{1}{\alpha}\left(\phi_{1\xi}\widetilde{b}_{1\xi} + \overline{Ha^2}\widetilde{\psi}_{1\xi}\widetilde{b}_0\widetilde{b}_{1\xi}\right) = -1 - \left(\frac{1}{2}\alpha - 1\right)\overline{Ha^2}\widetilde{\psi}_{1\xi}. \tag{75}$$

which means that the analytical side wall solution from section 3.1 is no longer valid for $Ha^2 = O(A^{-1})$.

For $Ha^2 = O(A^{-2})$, the primary flow in the core region will no longer be one-dimensional, as the equation for the core flow would read

$$\psi_{0yyyy} = \frac{1}{\alpha}\overline{Ha^2}\psi_{0x}bb_x = \overline{Ha^2}\left(1 + \alpha x\right)\psi_{0x}. \tag{76}$$

5. Numerical method

The presented analytic solution is, due to the underlying assumptions, strictly speaking valid only for small, but non-zero A and with Ha of at most $O(1)$, Ca of at most $O(A^4)$, Re of at most $O(A)$ and Bo of at most $O(A^2)$. In this section we will explore numerically the accuracy of the analytic expression as a function of the parameters A, Ha, Ca, Bo and Re by comparing the analytical results to the numerical simulations.

For the numerical simulation we use a finite volume based moving mesh interface tracking method, adapted from *interTrackFoam* of *OpenFOAM* distribution *1.6-extend*.

5.1. Moving mesh interface tracking method

The moving mesh interface tracking method is based on aligning a boundary of the numerical mesh with the free surface. This results in a sharp interface by definition and allows for the implementation of exact boundary conditions at the interface. The approach as proposed by Muzaferija and Perić [29] and the implementation by Ž. Tuković and Jasak [22] was used.

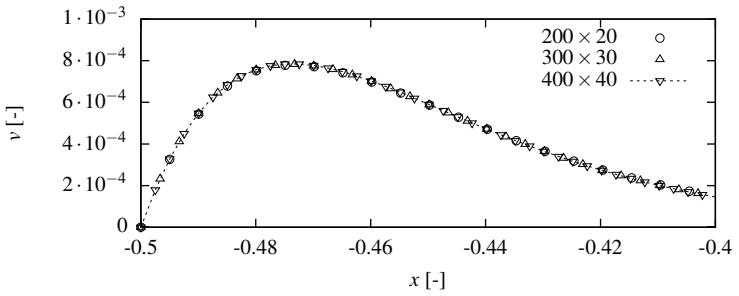

Figure 4: The vertical velocity component along the line $y = 0.5$ for $A = 0.1$, $Re = A$, $Ha^2 = 1$, $Bo = A^2$, $Ca = A^4$ for mesh resolutions of 200×20, 300×30 and 400×40.

The moving mesh interface tracking method introduces in addition to continuity and momentum equations the so called space conservation law, i.e.

$$\frac{d}{dt'} \int_{V'} dV' - \int_{S'} \hat{\mathbf{n}} \cdot \mathbf{v_s}' dS' = 0, \tag{77}$$

where $\mathbf{v_s}'$ is the velocity of the surface. This velocity of the surface of an arbitrary control volume V' has to be accounted for in the integrated mass and momentum conservation equations [29, 22]

The boundary conditions from section 2.2 do also apply for the numerical simulations, e.g. no mass should cross the boundary and the stresses at opposite sides of the interface should match. Non-zero mass fluxes through the free surface are corrected by moving the boundary. This correction is used as a boundary condition in the Laplace equation for moving the interior points in the domain by an amount $\mathbf{d}'$:

$$\nabla' \Gamma \cdot \nabla' \mathbf{d}' = 0 \tag{78}$$

where Γ is a diffusion parameter that in general is a function of the distance to the free surface. In this work, the diffusion parameter will be constant.

5.2. Details of numerical simulation

The simulations were performed on an initially square cell grid containing $(20/A) \times 20$ cells in the horizontal and vertical direction respectively, representing the bottom layer only. The convective term is discretized with a second order central differencing scheme, the time derivative with a second order implicit method and the least squares method was used for gradient calculation. For $A = 0.1$, $Ha^2 = 1$, $Ca = A^4$, $Re = A$ and $Bo = A^2$ and $\theta = 90°$ we show in figure 4 the velocity along the line $y = 0.5$ on the standard 200×20 mesh and 300×30 and 400×40 meshes, demonstrating the sufficient mesh resolution to capture the main flow structure, with the exception of the recirculations in the bottom corners. Velocities in these recirculations are orders of magnitude smaller than those of the main flow, and an infinity of ever decreasing recirculations is present, making the numerical capture of all recirculation flow details neither relevant nor feasible.

The numerical values for the material properties of the top phase are defined to be $\sigma_2/\sigma = 0$, $\rho_2/\rho = 0$ and $\nu_2/\nu = 0$, and are necessary for the boundary conditions, for example the pressure in the gas phase is assumed to be constant. The zero conductivity constraint for the top phase was implemented via the boundary condition for the electric potential at the interface, i.e. the normal gradient $d\phi/dn = \nabla \cdot (\mathbf{u} \times \mathbf{b})$. The contact angle boundary condition $\theta = 90°$, thus $m = 0$, was imposed on the side wall boundaries.

6. Numerical results

The analytical model was derived for $Re \leq O(A)$, $Ca \leq O(A^4)$, $Ha^2 \leq O(1)$, $Bo \leq O(A^2)$ and $A \to 0$. It predicts the surface elevation (equation 61), core flow (equation 44) and pressure (equation 45). For $A = 0.1$,$Re = A$, $Ha = 1$, $Bo = A^2$, $Ca = A^4$, $\theta = 90°$ and $\alpha = 1$, figure 5 compares the free surface elevation of the result from the numerical simulation with the analytical model for the first order deformation. It can be seen that the numerically determined free surface elevation is in good agreement with the analytical solution.

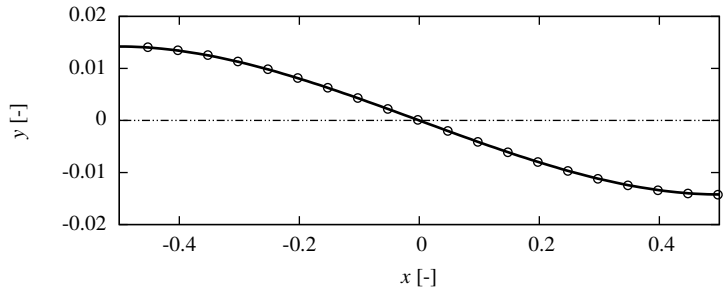

Figure 5: Elevation h_2 of the free surface over the width of the domain for $A = 0.1$, $Re = A$, $Ha^2 = 1$, $Bo = A^2$, $Ca = A^4$ and $\theta = 90°$. The numerical simulation (◯) and the first order analytic approximation (solid line) of equation 61 are shown.

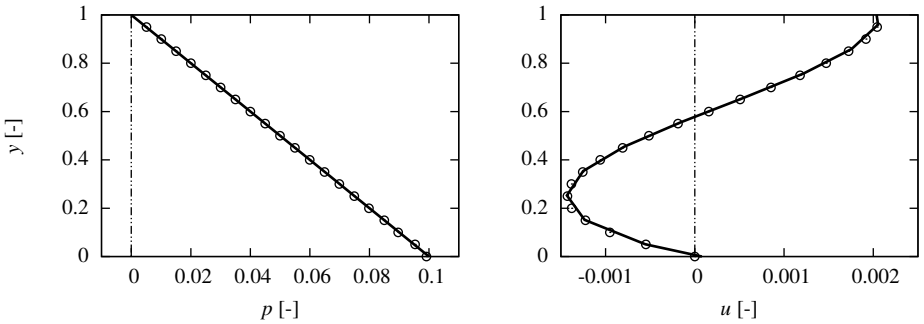

Figure 6: Modified pressure p_m (left) and horizontal velocity u (right) for the line $x = 0$ for $A = 0.1$, $Re = A$, $Ha^2 = 1$, $Bo = A^2$, $Ca = A^4$ and $\theta = 90°$. The numerical simulation (◯) and the first order analytic approximation (solid line) are shown.

For the same conditions, figure 6 shows the pressure (from equation 45, with $p(0, 1) = 0$) and horizontal velocity (from equation 44 and 19) for the vertical line $x = 0$. Again a good agreement is obtained between numerical simulations and analytic results.

In figure 7, again for the same conditions, both velocity components along the line $y = 0.5$ in the region close to the wall are depicted. The analytic solution is obtained from equation 72, with $P = 1024$. For both velocity components, it is seen that the velocity profiles obtained from the numerical simulation accurately match the analytical results.

6.1. Three-dimensionality of flow

In this section we will numerically show that the analytical derivation in a two-dimensional plane of the three-dimensional problem is valid. In the $z = 0$-plane, the Lorentz force has a zero component in the z-direction, therefore the three-dimensionality of the magnetic field does not influence the equations for u and v in that plane (equations 15 and 16). By introducing walls to bound the domain in the z direction, additional

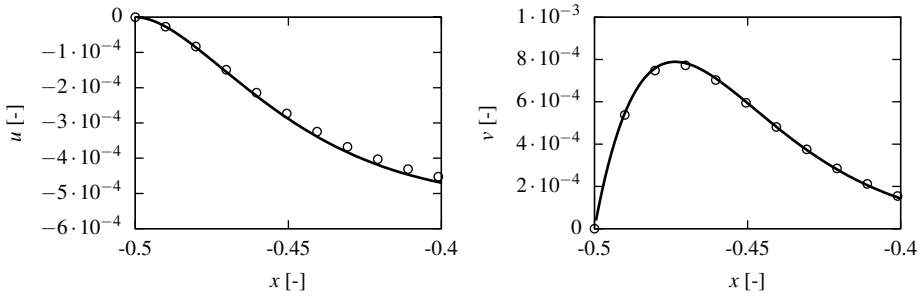

Figure 7: The horizontal (left) and vertical (right) velocity component along the line $y = 0.5$ for $A = 0.1$, $Re = A$, $Ha^2 = 1$, $Bo = A^2$, $Ca = A^4$ and $\theta = 90°$. The numerical simulation (◯) and the first order analytic approximation of equation 72 using $P = 1024$ for $y = 0.5$ (solid line) are shown.

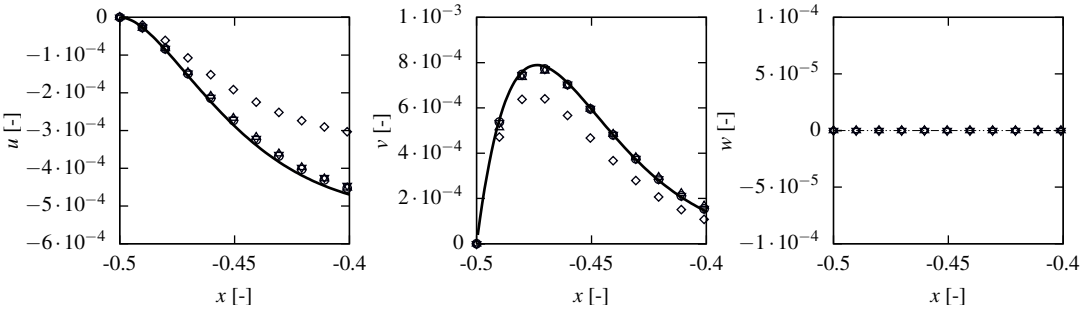

Figure 8: Horizontal (left) and vertical (middle) velocity components (as figure 7) and spanwise velocity component (right), along the line $y = 0.5$ for $A = 0.1$, $Re = A$, $Ha^2 = 1$, $Bo = A^2$, $Ca = A^4$ and $\theta = 90°$, for the analytical solution (solid line), the two-dimensional numerical simulation ($\bigcirc$), and the numerical simulation for a cavity with z-dimension $100d$ ($\triangle$), $10d$ ($\triangledown$) and d ($\Diamond$).

viscous shear from these walls can be expected. Figure 8 compares the velocity components for increasing size w of the domain in the z-direction. This size was consecutively increased from $w = d$, to $w = d/A$ and to $w = d/A^2$. For $w = d$, the velocities in the xy-plane are significantly smaller than analytically derived, whereas the shape of these velocity profiles has not changed. This is caused by the viscous shear from the walls that bound the domain in the z-direction. When the extend of the domain in the z direction increases, Figure 8 shows that the velocity profiles converge to the velocity profile from the two-dimensional numerical simulation and the analytical solution, without generating a significant velocity component in the spanwise direction. Therefore, the presented analytical solution is valid for the formulated three-dimensional problem.

6.2. Increased deformation

In this section we will obtain numerical results for the surface elevation under higher Hartmann number, capillary number, Bond number, Reynolds number and aspect ratio, in order to determine to what degree the analytic solution of equation 61 holds.

Figure 9 shows the free surface elevation for a set of cases in which, starting from $A = 0.1$, $\theta = 90°$, $Re = A$, $Ha^2 = 1$, $Ca = A^4$, $Bo = A^2$, either of the parameters Ha, Ca, Bo or A is increased to large values for which the analytic solution is not expected to hold.

From figure 9(a) it can be seen, that, even though the derivation for the free surface elevation is valid for $Ha^2 \leq O(1)$, the analytical solution using $Ha^2 = 1000$ still closely agrees with the numerical solution.

For capillary number increasing up to $Ca = 1000A^4$, the numerical solution slowly diverges from the analytical expression, as can be seen from figure 9(b), where both numerical and analytical free surface elevations are scaled with the capillary number. Although from a comparison between the boundary condition used with the present assumptions on Ca (equation 38) and the full boundary condition, (equation 27), it appears that for increasing values of Ca, the boundary condition gets increasingly complex. Figure 9(c) shows that for increasing Bo numbers, the free surface elevation quickly decreases, as does the surface curvature in the core, in line with equation 61. The analytical model fits the numerical data surprisingly well. Finally, figure 9(d) shows that for an aspect ratio as large as $A = 0.5$, the analytically determined free surface elevation is still matching the numerical result very well.

A quantitative analysis of the accuracy of the analytical model for increasing Ha^2, Ca. Bo, Re and A is shown in figure 10, which shows the normalized root mean square distances between the analytically calculated elevation (equation 61) and the numerically calculated elevation, normalized by $\int h^2 dx$. This distance is a measure for the deviation of the analytical result from the numerical simulation.

For $A \leq 0.1$, $Ha^2 \leq 1$, $Ca \leq A^4$, $Bo \leq A^2$ and $Re \leq A$, the error in the analytical solution of the free surface elevation, compared to the numerical solution, is less than 0.4%. Keeping all the other parameters fixed, this error increases to $\sim 1\%$, when either Ha^2 is increased to ~ 400, Ca to $\sim 200A^4$ or Bo to $\sim 100A^2$, whereas the error stays well below 1% when Re is increased to $10^3 A$. For $Ha^2 \leq 1$, $Ca \leq A^4$, $Bo \leq A^2$, $Re \leq A$, the error remains less than 1% for $A = 0.2$ and less than 2% for $A = 0.5$.

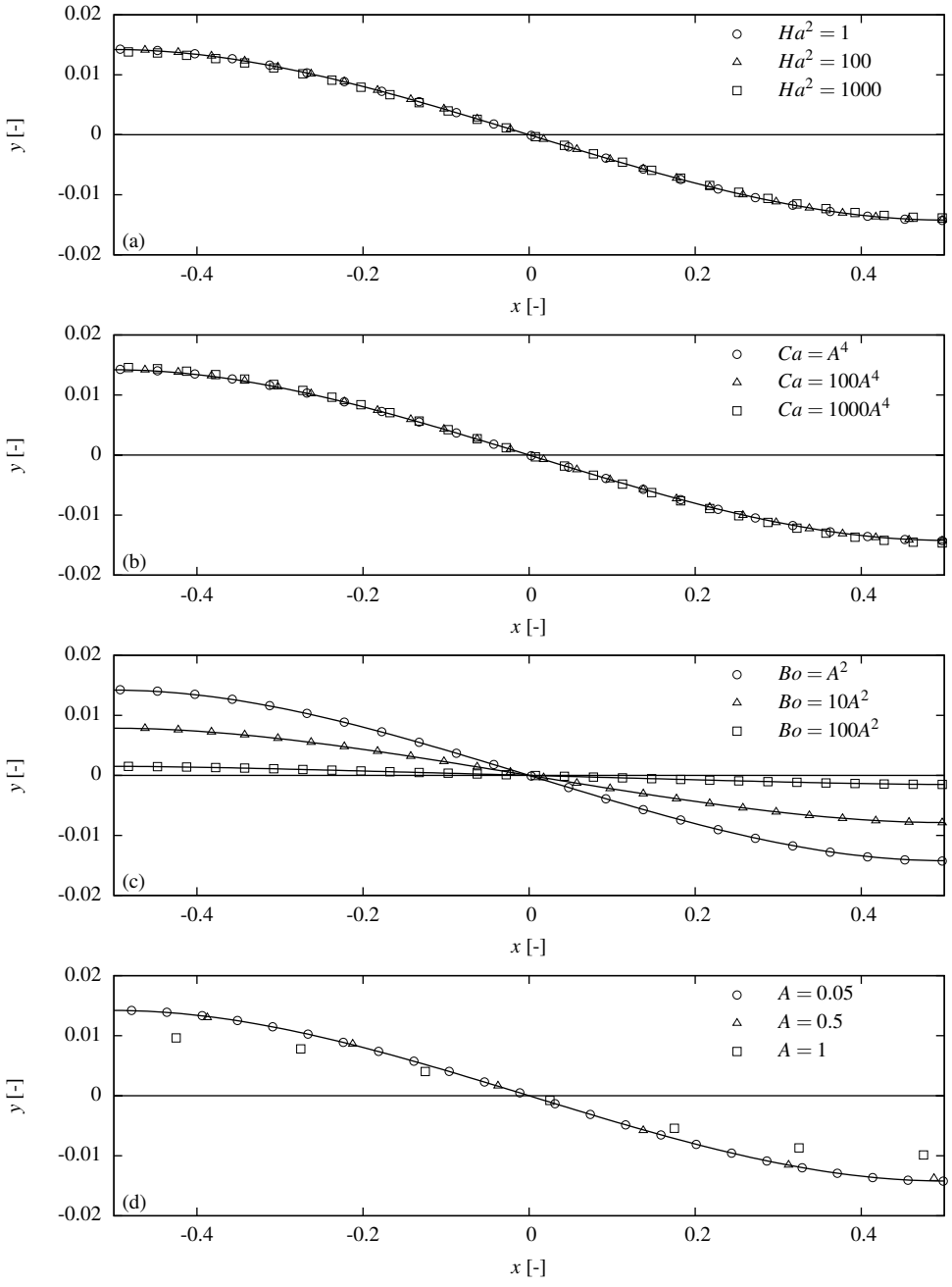

Figure 9: The surface elevation h_2 from the MMIT simulations (symbols), horizontally rescaled to $[-0.5, 0.5]$, where from $A = 0.1$, $Ha^2 = 1$, $Ca = A^4$, $Bo = A^2$, either of the parameters Ha^2 (a), Ca (h rescaled by $\overline{Ca}$) (b) , Bo (c) and A (d) is increased. The solid line indicates the analytic solution (equation 61) for $\overline{Ca} = \overline{Bo} = 1$ and the dashed lines for $\overline{Bo} = 10$, $\overline{Bo} = 100$ respectively.

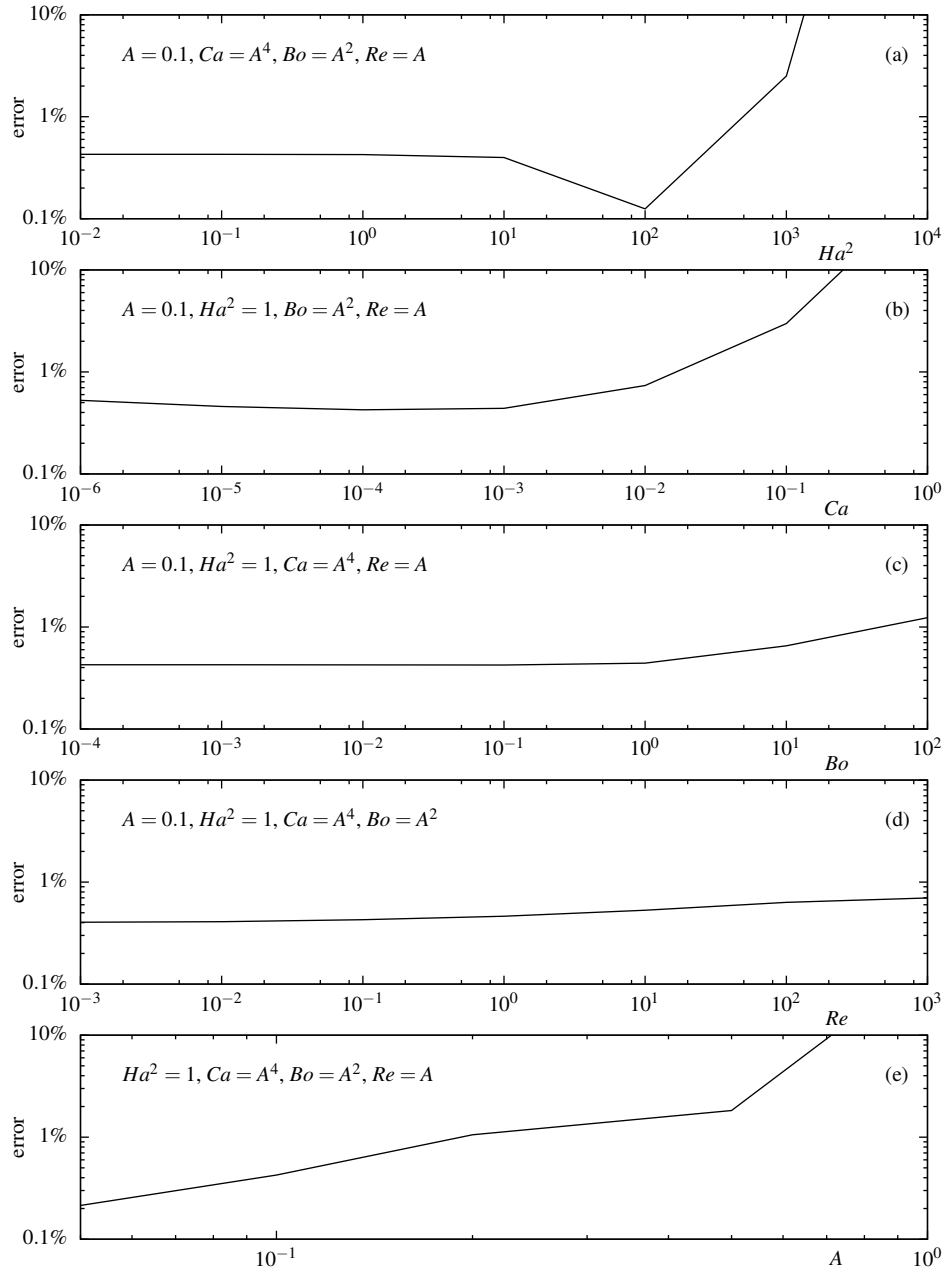

Figure 10: The normalized root mean square distance between the surface elevation profile from the numerical simulation and the analytical free surface elevation, where from the case $A = 0.1$, $Re = A$, $Ha^2 = 1$, $Bo = A^2$ and $Ca = A^4$, either (from top to bottom) Ha^2, Ca, A, Re or Bo is varied. The root mean square distance is normalized with $\int h^2(x)dx$.

7. Discussion and conclusion

In this paper we have studied the flow and free surface elevation of a layer of conductive liquid with height-to-width ratio $A \ll 1$, that is subject to a potential difference horizontally across the domain and a traverse x-dependent magnetic field. It was shown that the surface tension and gravity forces in combination with the unevenly distributed Lorentz forces on the fluid induce a steady state flow, which scales linearly with conductivity, magnetic field gradient and applied potential difference and which vanishes for infinitely long layers ($A \to 0$), whereas the free surface deformation depends on the capillary number, the Bond number and the contact angle condition.

Increasing pressure within the layer will cause the interface to deform. The profile of this interface was derived analytically for Hartmann numbers up to $O(1)$, capillary numbers up to $O(A^4)$, Bond numbers up to $O(A^2)$ and Reynolds numbers up to $O(A)$, while $A \ll 1$. It was proven that to lowest order approximation, the surface elevation profile is a function of the capillary number, the Bond number and the contact angle condition. The magnitude of the free surface displacement scales linearly with the capillary number and decreases with increasing Bond number. The shape of the free surface is determined by both the Bond number and the contact angle boundary condition.

Furthermore, the biharmonic equation for the stream function in the side wall region was solved analytically, showing the turning of the flow and the presence of small eddies in the corner regions.

The first order approximation of the analytic solution was confirmed with a finite volume computational model for free surface flow simulation using a moving mesh interface tracking technique in combination with a one-way coupled MHD solver via the equation for the electric potential. The analytically derived elevation and subsurface flow properties match the numerical simulation well.

Using numerical simulations, it is observed, that for larger values of the Hartmann number, capillary number, Bond number, Reynolds number and aspect ratio, where the underlying assumptions of the analytic solution are no longer satisfied, the analytical solution and numerical results match reasonably well, within 1%, for $A = 0.1$ and either Ha^2 up to 400, Ca up to $200A^4$ or Bo up to $100A^2$ and is accurate within 2% for $A = 0.5$.

The analytical solution presented in the present paper is derived up to $O(A)$. This means that the lowest order neglected terms are of order $O(A^2)$. For small enough aspect ratio ($A = 0.1$) these terms quickly reduce to values smaller than 1%. Indeed, the difference with the numerically found solution is only 0.4% for $A = 0.1$. We therefore conclude that the contribution of the neglected higher order terms in the analytical solution, for an aspect ratio of 0.1, is smaller than 1%.

Acknowledgements

This work was supported by the Dutch Technology Foundation STW, grant 10488, Tata Steel, and ABB.

References

[1] S. Oshima, R. Yamane, Shape-control of Liquid Metal Free Surfaces by Means of a Static Magnetic Field, in: J. Szekely, J. W. Evans, K. Blazek, N. El-Kaddah (Eds.), Magnetohydrodynamics in Process Metallurgy, The Minerals, Metals and Materials Society, 251–259, 1991.

[2] P. Gillon, Materials processing with high direct-current magnetic fields, JOM 47 (5) (1995) 34–37.

[3] Y. Fautrelle, A. D. Sneyd, Instability of a plane conducting free surface submitted to an alternating magnetic field, Journal of Fluid Mechanics 375 (1998) 65–83.

[4] A. Juel, T. Mullin, H. Ben Hadid, D. Henry, Magnetohydrodynamic convection in molten gallium, Journal of Fluid Mechanics 378 (1999) 97–118.

[5] R. W. Series, D. T. J. Hurle, The use of magnetic fields in semiconductor crystal growth, Journal of Crystal Growth 113 (12) (1991) 305–328.

[6] J. Garandet, T. Alboussière, Bridgman growth: Modelling and experiments, Progress in Crystal Growth and Characterization of Materials 38 (1) (1999) 73–132.

[7] J. A. Shercliff, The Flow of Conducting Fluids in Circular Pipes Under Transverse Magnetic Fields, Journal of Fluid Mechanics 1 (06) (1956) 644–666.

[8] J. C. R. Hunt, Magnetohydrodynamic Flow in Rectangular Ducts, Journal of Fluid Mechanics 21 (04) (1965) 577–590.

[9] T. Alboussière, J. P. Garandet, R. Moreau, Asymptotic analysis and symmetry in MHD convection, Physics of Fluids 8 (8) (1996) 2215–2226.

[10] W. Bian, P. Vasseur, E. Bilgen, Effect Of An External Magnetic Field On Buoyancy-driven Flow In a Shallow Porous Cavity, Numerical Heat Transfer, Part A: Applications 29 (6) (1996) 625–638.

[11] H. Ozoe, K. Okada, The effect of the direction of the external magnetic field on the three-dimensional natural convection in a cubical enclosure, International Journal of Heat and Mass Transfer 32 (10) (1989) 1939–1954.

[12] L. Davoust, M. D. Cowley, R. Moreau, R. Bolcato, Buoyancy-driven convection with a uniform magnetic field. Part 2. Experimental investigation, Journal of Fluid Mechanics 400 (1999) 59–90.

[13] W. F. Hughes, R. A. Elco, Magnetohydrodynamic lubrication flow between parallel rotating disks, Journal of Fluid Mechanics 13 (01) (1962) 21–32.

[14] B. Lehnert, An Instability of Laminar Flow of Mercury Caused by an External Magnetic Field, Proceedings of the Royal Society of London. Series A, Mathematical and Physical Sciences 233 (1194) (1955) 299–302.

[15] E. F. Northrup, Some Newly Observed Manifestations of Forces in the Interior of an Electric Conductor, Physical Review (Series I) 24 (6) (1907) 474–497.

[16] A. Kharicha, I. Teplyakov, Y. Ivochkin, M. Wu, A. Ludwig, A. Guseva, Experimental and numerical analysis of free surface deformation in an electrically driven flow, Experimental Thermal and Fluid Science 62 (2015) 192–201.

[17] K. Sundaravadivelu, P. Kandaswamy, K. Kumar, Effect of magnetic field on the liquid-gas interfacial deformation in thermocapillary convection problem, Zeitschrift für angewandte Mathematik und Physik 51 (3) (2000) 491.

[18] D. Cormack, G. Stone, L. Leal, The effect of upper surface conditions on convection in a shallow cavity with differentially heated end-walls, International Journal of Heat and Mass Transfer 18 (5) (1975) 635–648.

[19] A. K. Sen, S. H. Davis, Steady thermocapillary flows in two-dimensional slots, Journal of Fluid Mechanics 121 (1982) 163.

[20] J. Garandet, T. Alboussière, R. Moreau, Buoyancy driven convection in a rectangular enclosure with a transverse magnetic field, International Journal of Heat and Mass Transfer 35 (4) (1992) 741–748.

[21] H. Ben Hadid, D. Henry, Numerical study of convection in the horizontal Bridgman configuration under the action of a constant magnetic field. Part 2. Three-dimensional flow, Journal of Fluid Mechanics 333 (1997) 57–83.

[22] Ž. Tuković, H. Jasak, A moving mesh finite volume interface tracking method for surface tension dominated interfacial fluid flow, Computers and Fluids 55 (2012) 70–84.

[23] P. A. Davidson, An Introduction to Magnetohydrodynamics, Cambridge University Press, 1 edn., ISBN 0521794870, 2001.

[24] D. E. Cormack, L. G. Leal, J. Imberger, Natural Convection in a Shallow Cavity with Differentially Heated End Walls. Part 1. Asymptotic Theory, Journal of Fluid Mechanics 65 (02) (1974) 209–229.

[25] F. Verhulst, Methods and Applications of Singular Perturbations, Springer Science+Business Media, Inc., 1 edn., 2005.

[26] J. Benthem, A Laplace transfor method for the solution of semi-infinte and finite strip problems in stress analysis, Quarterly Journal of Mechanics and Applied Mathemathics 16 (4) (1963) 413–429.

[27] M. H. Meylan, L. Gross, A parallel algorithm to find the zeros of a complex analytic function., ANZIAM Journal 44 (0) (2003) E236—E254.

[28] H. K. Moffatt, Viscous and resistive eddies near a sharp corner, Journal of Fluid Mechanics 18 (01) (1964) 1–18.

[29] S. Muzaferija, M. Perić, Computation Of Free-Surface Flows Using The Finite-Volume Method And Moving Grids, Numerical Heat Transfer, Part B: Fundamentals 32 (4) (1997) 369–384.